The Influence of Central Supermassive Black Holes on Major Merger Remnants

David Schlachtberger

Munich 2011

The Influence of Central Supermassive Black Holes on Major Merger Remnants

Bachelor Thesis

at the

Ludwig–Maximilians–Universität (LMU) München

submitted by

David Schlachtberger

(Matr. Nr.: 10108076)

born on April 27, 1988 in Starnberg

supervised by

Prof. Dr. Andreas Burkert

and

Rhea-Silvia Remus

Munich, July 19, 2011

Evaluator: Prof. Dr. Andreas Burkert

Contents

1 Introduction

It is well known from observations that two of the most common structures in the universe are spiral- and elliptical galaxies. They are both gravitationally bound systems containing luminous, gaseous and dark matter, but differ in shape. Spiral galaxies, like the Milky Way, are relatively thin disks with a pronounced internal spiral structure, whereas elliptical galaxies are generally smoother with a rounder shape. There is evidence that the collision of two spiral galaxies may form elliptical galaxies by so called major mergers (Hernquist, 1992). During these dynamically violent events, the involved spirals are redistributed into a more homogeneous elliptical shape.

Observations have shown that the centers of many galaxies contain supermassive black holes (BHs), dark objects not bigger than a few parsec (pc) but with masses of $10^6 - 10^9$ times the mass of the sun ($M_\odot$). The BHs can get so heavy by accreting gas onto them. In a spiral galaxy this process usually stops once the BH accreted all the gas within its range of influence. But if the galaxy undergoes a major merger, the gas gets redistributed and usually accumulates in the center. During this event, the two involved BHs can also merge into one even more massive BH. It is surrounded by a high density of gas so that the accretion rate is high, which leads to the release of a large quantity of accretion energy. This feedback process is not yet fully understood, but observations have shown that a significant fraction of the accreted mass is converted into thermal energy that gets injected into the the surrounding gas (Binney and Tremaine, 2008, p. 764). This indicates that BH feedback is an important impact on a galaxy.

Due to their small size, BHs are difficult to detect. Only in the Milky Way and a few other nearby galaxies this could be achieved directly by dynamic measurements of stars in the proximity of the BH (Kormendy and Richstone, 1995). The resolution requirements of this method are too high for galaxies that are further away. Therefore it is necessary to examine the interactions between the BHs and their hosts with the help of simulations in order to find resolvable features in the galaxies than can indicate properties of the BH. The data collected from such simulations allow detailed analyses of the features of interest, such as radial mass distribution and dynamical properties. This was done in this thesis.

2 Data Analysis

In the course of this work high resolution simulations of elliptical galaxies created in a major merger event were analyzed. At first, the simulation codes used by Johansson et al. (2009a) will be reviewed, followed by a presentation of the methodology employed in this work to analyze the simulations.

2.1 Simulations

The simulations that were examined in this thesis were presented by Johansson et al. (2009a). They were computed with the TreeSPH-code GADGET-2 by Springel (2005). This type of code uses Smoothed Particle Hydrodynamics (SPH), a technique that combines all physical particles within a certain Smoothing Length ϵ into one numerical particle, which is then attributed with the smoothed properties (e.g. the potential, velocity, etc.) of all the combined particles. One the one hand, this limits the numerical resolution to ϵ (e.g. Monaghan, 1992), but on the other, it suppresses unphysical events like inelastic collisions of stars. Another advantage is that it can be formulated in a way that guaranties energy and entropy conservation (Johansson et al., 2009b).

Most of the simulations that are studied here contain a component of gas particles. The gas consists of a primordial mixture of hydrogen and helium. It can be cooled via radiative cooling down to $10^4 K$. The physical background for this kind of cooling is that the particles in a gas cloud excite each other by collisions, then they relax via emission of a photon, which can carry energy out of the cloud. This is only effective for temperatures above $10^4 K$ in a relatively dense cloud, so the gas can only get colder than that by adiabatic expansion (see section 3.3.2).

Star formation is simulated by the mutation of a numerical gas particle into a newly formed star particle of the same mass. In this process the gas particle turns gradually into a star particle following the sub-resolution model of Springel and Hernquist (2003) and is eventually considered to be a star particle once 50% of it is stellar matter. During star formation, the particle release supernova feedback energy into the surrounding gas and heat it.

In the simulations the central supermassive black hole (BH) acts as a sink for gas particles. For each particle, 0.5% of the accreted energy is injected into the surrounding gas as thermal energy, so this feedback energy increases as more gas gets absorbed. Above a threshold accretion rate, the feedback becomes so strong that it blows away all surrounding gas within a certain radius. (Johansson et al., 2009a)

Model No.	Mass Ratio	$f_{gas}[\%]$	BH	Bulge	$M_{BH}[10^7 M_\odot]$
11B2Bu	1:1	20	yes	yes	4.6
11nB0Bu	1:1	0	no	yes	0
11B2nBu	1:1	20	yes	no	9.1
11nB0nBu	1:1	0	no	no	0
31B8Bu	3:1	80	yes	yes	6.7
31B2Bu	3:1	20	yes	yes	2.7
31nB2Bu	3:1	20	no	yes	0
ESp2	E-Sp	20	yes	yes	5.0

Table 2.1: Main parameters of the examined simulations; f_{gas} = initial faction of gas in the galaxy disk; M_{BH} = final mass of the BH

The BH positions are calculated using the BH repositioning method of Johansson et al. (2009b), where each BH particle is at each time step repositioned to the point of the deepest potential in the area. This prevents ejection of the BHs during the merger and ensures effective BH merging once both are within the smoothing length of each other and move sufficiently slow (Johansson et al., 2009a).

The progenitor spiral galaxies are set up using the method of Springel (2005) with parameters similar to those of the Milky Way. At first a dark matter halo with a Hernquist (1990) profile is set up with typical parameters for a present day ($z = 0$) galaxy. The halo is then populated with an exponential disk with a gas fraction f_{gas} and the rest being stars. Then an extra bulge component with total mass $m_{bulge} = 1/3 m_disk$ is added. Finally a relatively small seed BH with $m_{BH} = 10^5 M_\odot$ is inserted in the center of the galaxy (Johansson et al., 2009a).

Pairs of simulations are run with almost identical initial conditions only differing in the absence of one or two components. Especially the runs with and without seed BHs were important for the present paper since the influences of a central BH on the major merger evolution were to be studied. One set of simulations was run with two equal mass (1:1) progenitors. To simulate unequal mass mergers, all particle numbers of one of the two galaxies were scaled down by a factor of 3, resulting in the 3:1 merger series. In addition, a consecutive merger scenario was simulated where an elliptical galaxy, which was the remnant of an 1:1 spiral merger, merged with another full spiral galaxy. The studied combinations of mass ratio, initial gas content f_{gas}, presence of a BH, and a bulge component are summarized in table 2.1.

The numerical resolution of these simulations was relatively high as each standard progenitor galaxy had 300,000 disk particles including the gas particles, 100,000 bulge particles and 400,000 dark matter halo particles. The gravitational softening length, which determines the numerical resolution, was set to $\epsilon = 0.02 h^{-1}$ kpc ≈ 0.028 kpc for all baryonic particles and the BHs and to $\epsilon = 0.086 h^{-1}$kpc for the dark matter particles. Here, $h = 0.71$ is the coefficient of the Hubble Parameter $H_0 = h \times 100\text{km s}^{-1}\text{Mpc}^{-1}$. (Johansson et al., 2009a)

The orbital geometry for all mergers is G13 based on Naab and Burkert (2003).

Here, the galaxies approach each other on parabolic orbits with a small offset of the pericenters. The spiral galaxies are inclined relative to the orbit plane, with an inclination of $i_p = -109°$ and $i_s = 180°$ for the primary and secondary galaxy, respectively. The simulations are evolved for a total of $t = 3$ Gyrs each, with the merger typically taking place at $t \approx 1.5$ Gyrs. The main parameters of the 8 analyzed simulations are summarized in table 2.1. For further details on the simulations, see Johansson et al. (2009a).

2.2 Methodology

The results of the above reviewed simulations were available for this work as raw data that contained information about the position and velocity of all particles. The data also included additional information on special properties of some kinds of particles like for example the temperature of each numerical gas particle. The analysis of the raw data was done with the computer program IDL using the methods described below.

For this thesis only the last snapshot of each simulation was analyzed, which represented the state of the galaxy after 3 Gyrs, which is about 1.5 Gyrs after the merger. At this point the violent merging event was completed and the remnant already relaxed in the inner parts.

The simulations distinguish between different kinds of particles, e.g. disk, bulge, and newly formed stars, which together represent the luminous matter (lum). Most of the time the plots here will not refer to the individual types but treat them as entity. The gas particles are treated separately and are marked accordingly. The dark matter halo particles are largely ignored except for the calculation of the rotation curve (see section 2.2.3).

In all profile plots the radius was plotted logarithmically from $r_{min} = 0.02h^{-1}$ kpc $= 0.028$ kpc, which is the numerical resolution, to 100 kpc.

2.2.1 Visible Structures

The projection plots (section 3.1.1) display the spatial positions of the luminous and the gas particles relative to the gravitational center of the galaxy. There are three orthogonal projections representing the principal axis of the luminous matter distribution of the inner 50% of the luminous particles. The gas particles are projected using the same principal axis as for the luminous matter. The projections are calculated from all particles within a 3D-cube around the center with the labeled edge length in all three directions.

2.2.2 Binned Plots (Density, Velocity Dispersion, Anisotropy Parameter)

For the density, velocity dispersion, and anisotropy parameter profiles (sections 3.1.2, 3.2.1 and 3.2.2), the particles were radially binned so that each bin contained the next n_p particles that were closest to the center.

The density in a bin ρ_{bin} was calculated by adding all masses inside the spherical shell and then dividing the result by the volume of the shell.

$$\rho_{bin} = (\sum_{bin} M) / \left(\frac{4}{3} \pi \left(r_{max}^3 - r_{min}^3 \right) \right) \tag{2.1}$$

The velocity dispersion σ_{bin} is the standard deviation of all 3-dimensional velocity vectors (bars are for the mean of the value):

$$\sigma_{bin} = \sqrt{(\overline{v_x^2} - \overline{v_x}^2) + (\overline{v_y^2} - \overline{v_y}^2) + (\overline{v_z^2} - \overline{v_z}^2)} \tag{2.2}$$

The anisotropy parameter β is defined in spherical coordinates as in Binney and Tremaine (2008, p. 294) (bars are for the mean of the value):

$$\beta = 1 - \frac{\overline{v_\theta^2} + \overline{v_\phi^2}}{2\overline{v_r^2}} \tag{2.3}$$

If the mean squares of the tangential and the radial velocity components are identical, then $\overline{v_\theta^2} + \overline{v_\phi^2} = 2\overline{v_r^2}$ and $\beta = 0$. In that case, the galaxy is called isotropic, which means that the directions of motion of the particles are randomly distributed and no direction is preferred. In a tangentially biased system the anisotropy parameter is negative, and $\beta = -\infty$ for perfectly round orbits, because the radial velocity component vanishes, so $\overline{v_r^2} = 0$. If a system is radially dominated, all particles fly away from or towards the center, thus the tangential motion vanishes and $\beta = 1$, since $\overline{v_\theta^2} + \overline{v_\phi^2} = 0$.

Due to the high resolution and relatively low particle numbers close to the center, the bin size was chosen to be $n_p = 100$ for the density profiles and $n_p = 1000$ for the others. The density profile was then smoothed over 3 and 15 points for the luminous matter and the gas respectively. The radius plotted for each bin is the midpoint of the smallest and the biggest radius in each bin.

Line of Sight

To obtain comparability with observational data, line-of-sight (l.o.s.) profiles for the density and velocity dispersion were computed (section 3.1.2 and 3.2.1). For that purpose, binning was no longer spherical but cylindrical around two different principal axes respectively. The particle numbers per bin were set to $n_p = 1000$. One of the chosen cylinder axes coincided with the axis of the central gas disk, therefore

the gas disk could be studied face-on. The other chosen axis was perpendicular to the first one, thus it lay in the disk plane and provided a edge-on view. The line-of-sight density is simply the density in each cylinder shell whereas the line-of-sight velocity dispersion is computed using only the velocity components parallel to the line of sight.

2.2.3 Cumulative Mass Plots (Mass Curve, Rotation Curve)

The mass and rotation curves (section 3.1.3 and 3.1.4) were plotted using the cumulative mass $M(< r)$ inside the given radius r from the center. The mass curve only took into account the luminous matter and gas respectively. To depict the effect of the newly formed stars, the mass curves of only the residual, that is the disk and bulge particles, were plotted as well. In the rotation curve the mass of all luminous, gas, and dark matter particles was added up. The rotation velocity v_{rot} was then calculated.

$$v_{rot}(r) = \sqrt{\frac{GM(< r)}{r}} \tag{2.4}$$

Here, r is the distance from the center, $M(< r)$ is the total mass inside r, and $G = 4.3 \times 10^{-6}$ kpc $M_{\odot}^{-1}(km/s)^2$ is the gravitational constant (Binney and Tremaine, 2008, p. 14).

Missing gas mass estimates

The simulations with a central BH had less gas in the center than those without a BH. The mass of the missing gas particles was graphically estimated using the mass curves. That was only possible for the 3:1, 20% gas mergers in a direct way because it was the only pair of simulations that contained gas in the version without BH. Figure 2.1 illustrates for this case how the possible range of radii near 0.7 kpc for the gas hole were estimated. Subsequently the corresponding cumulative gas masses for the case when no BH was present were determined, thus giving an estimate for the mass that is missing.

In all other cases the gas curves had to be estimated for the BH-less case. This was done by assuming that the curve in the 3:1, 20% gas, no BH simulation has typical characteristics. These are to decrease linearly from about 10 kpc inwards with a slightly smaller slope that the galaxies with a BH. The estimated mass curve for the gas in the 3:1, 80% gas simulation if the BH is missing is shown in figure 2.1 as light blue line. Using this curve, the missing gas masses were then approximated with the same technique as described above. Due to all the uncertainties of this method the estimates can only be seen as very rough first approximations with potentially large errors. The details of figure 2.1 are studied in section 3.1.3.

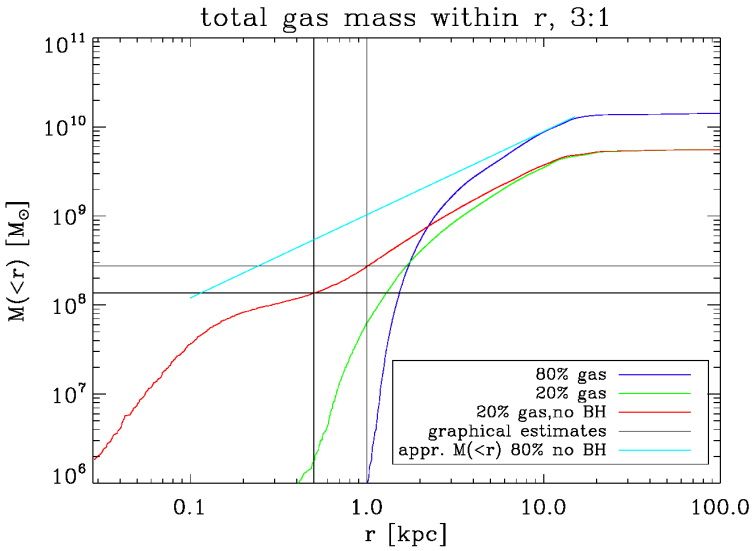

Figure 2.1: Graphical estimates of the missing gas mass (black lines) and approximation of the gas curve for the unavailable 80% gas, no BH case (light blue)

2.2.4 Vector Plots

Finally, the dynamics of the gas particles were studied. For this purpose, the spatial distribution of the gas was plotted again, but now with small vectors indicating the velocity of each particle in the plotting plane. Additionally, the vectors were colored to show various properties, namely the magnitude and direction of the radial velocity component v_r of the gas, the temperature of the gas particles divided into hot and cold gas at the border temperature of 10^4 K, and the age of the newly formed stars in Gyrs after the beginning of the simulation divided at 1.5 Gyrs, the approximate time of the merger event. The colors are plotted going from light to dark and sorted by color so that all blue colors are plotted over all red colors or vice versa as indicated in the legend.

3 Results

The interaction of an elliptical galaxy with its central super massive black hole (BH) can be analyzed in different ways. The first important characteristic that was examined here is the spatial distribution of the luminous and gaseous matter. Next, the influence of the BH on the dynamical properties of the galaxies is described. The BH had an significant impact on the gas in an ellipse, therefore the last part focuses on some special properties of the gas.

3.1 Mass Distributions

Stars and gas define the directly detectable structure of an elliptical galaxy and also interact with the central BH. Therefore, the analysis of the mass distribution helps to understand the properties of the galaxy and indicates influences of the BH.

3.1.1 Visible Structures of the Remnants

The analysis of the data began with a visualization of the major merger remnant. Figure 3.1 illustrates the luminous matter distribution projected to a principal axes system. The figure shows that merging of two disk galaxies similar to the Milky Way resulted in a galaxy with an elliptical shape (as predicted by Hernquist, 1992). The remnant appeared roundest in the upper left panel but even there it was slightly prolonged along one axis (the Z axis in most cases). This will be relevant for the study of the gas movement in section 3.3.1. The lower right panel of figure 3.1 is a zoom-in of the upper left panel and shows both that the position of the BH is very close to the gravitational center and that the density is highest in the center, as expected (e.g. Johansson et al., 2009b).

Figures 3.2 and 3.3 display the gas distribution in the same coordinate system as for the luminous matter above. One can see a defined gas disk that survived the merger. In the 1:1 merger simulation with bulge component (fig. 3.2a) this disk was relatively strongly disturbed due to the greater turbulence in equal mass mergers (Johansson et al., 2009b) resulting in a very small disk inside a dense, diffuse cloud. In the same galaxy, only without a bulge component (fig. 3.2b), the gas is not so diffuse and there are two concentric gas rings that are almost perpendicular to each other. This probably resulted from the fact that the two progenitor disks were also at an angle.

The 3:1 mergers (fig. 3.3) were less violent, resulting in a relatively well conserved disk that most likely belonged to the more massive progenitor. Some tidal tails,

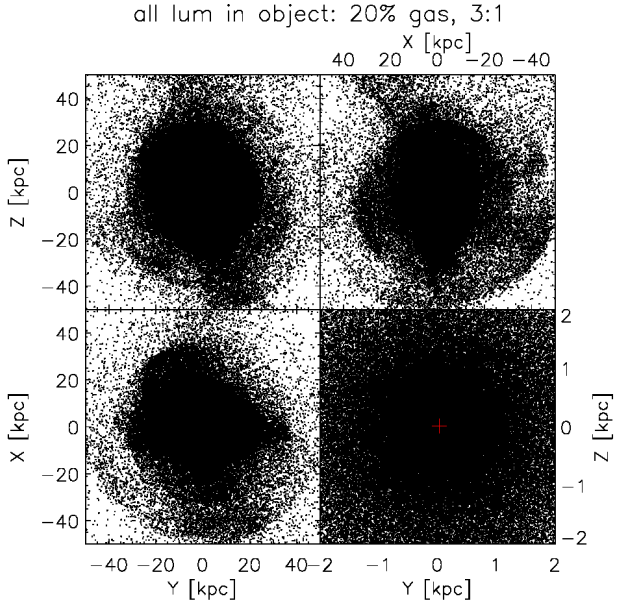

Figure 3.1: Projection of the star distribution in the 3:1, 20% gas merger remnant along the principal axes. The lower right panel is a scale-up of the center of the upper left one. The BH position is marked with a red cross.

which are spiral arms that were dragged out of the disk plane, can be seen as a result of the merger, but to a large extend the disk characteristic is still intact.

An important feature of all galaxies with a central BH (fig. 3.2 and 3.3a) is illustrated in the lower right panels, which are a scale-ups of the center of the galaxy. Inside the central 2 kpc a well defined hole in the gas disk with radii between 0.5 kpc and 1 kpc can be seen. In contrast, with the central BH missing (fig. 3.3b) there also is no hole but a dense clump of gas in the center. This indicates that the BH feedback blew out a considerable amount of gas from the center. This amount will be estimated in section 3.1.3.

3.1.2 Density Profiles

The density profiles of the luminous matter and gas in the 3:1 simulations can be found in figure 3.4. The profiles are linear from about 1 kpc to 30 kpc on a double logarithmic plot indicating a power law profile. Inside approximately 0.5 kpc the slope increases relative to the outer linear part with the increase being proportional to the gas fraction. Thus, without gas the slope does not get steeper whereas the 3:1, 80% gas merger (fig. 3.4, blue) has the most pronounced raise. This is in accordance with the theory that gas-rich mergers have extra central components that are missing in mergers without gas (Kormendy and Bender, 2009; Kormendy et al., 2009). The strong correlation with the gas content indicates that newly formed stars moved to the center or, more likely, mainly formed there.

Inside approximately 0.1 kpc the slope hardly decreases if no BH was included (fig. 3.4, red), but if a BH was present, the density is nearly constant all the way to the center. This is a significant feature that was caused solely by the BH. This was

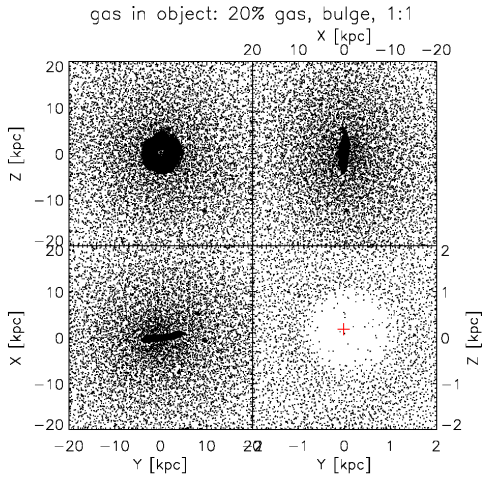

(a) 1:1 merger with bulge.

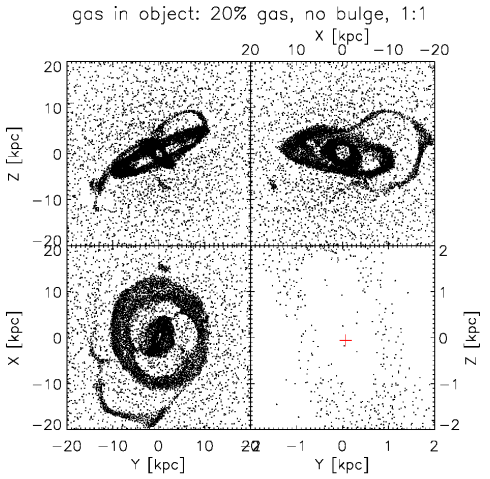

(b) 1:1 merger without bulge.

Figure 3.2: Projections of the gas in the 1:1 mergers with and without bulge. The lower right panel is a scale-up of the center of the upper left one. The BH position is marked with a red cross.

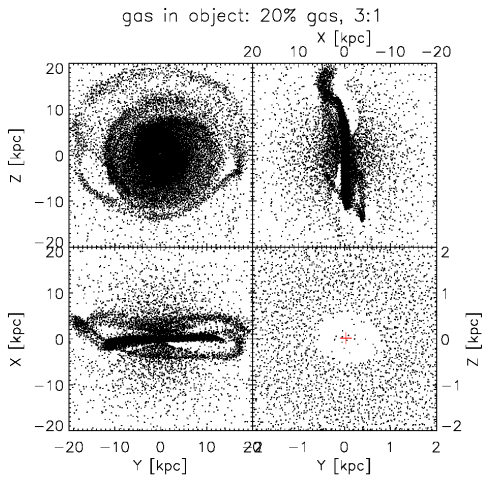

(a) 3:1 merger with BH.

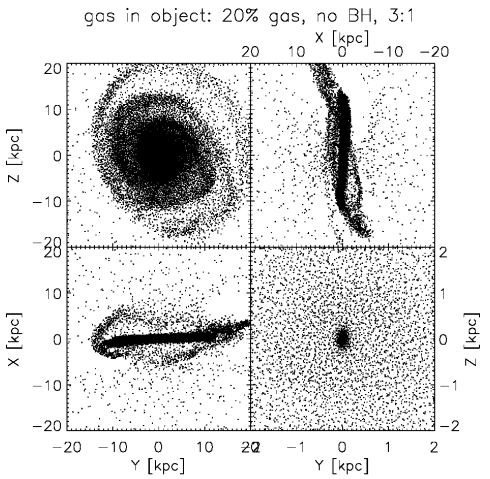

(b) 3:1 merger without BH.

Figure 3.3: Projections of the gas in the 3:1, 20% gas mergers with and without BH. The lower right panel is a scale-up of the center of the upper left one. Note that there is a hole in the center of the disk of the merger with BH and a clump without BH.

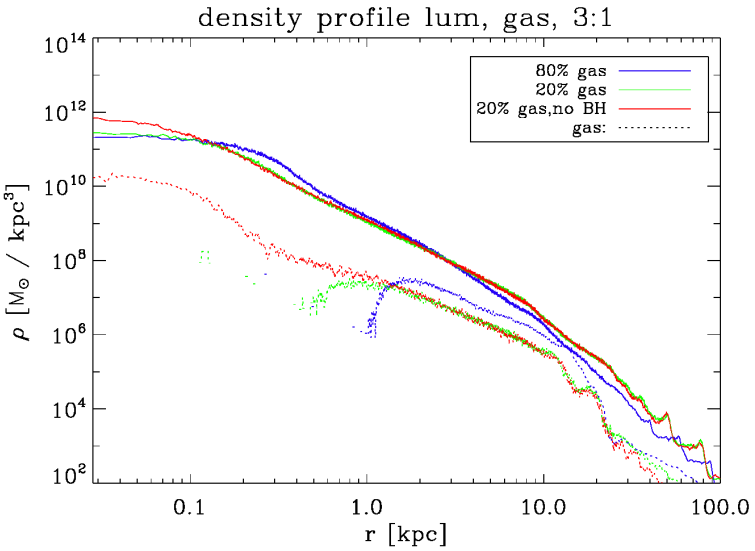

Figure 3.4: The radial density profiles of the 3:1 mergers for luminous and gaseous matter.

the BH's only impact on the luminous matter density profile and it was limited to the inner 0.1 kpc in a 3:1 merger, since the red (no BH) and green (with BH) lines in figure 3.4 only differ in this region. The comparison of the green (20% gas) and the blue (80% gas) line in figure 3.4 suggests that the radius at which the density becomes constant is correlated with the BH mass and/or the primal gas content. These values are both higher in the 80% gas simulation, so this radius is larger there as well.

The gas density profiles, plotted as a dashed lines, also show a distinct influence of the BH. As expected from the projection plots (section 3.1.1), the density first decreases strongly and then vanishes at radii between 0.5 kpc and 1 kpc following the hole structure seen before. This is again only true for the galaxies with a central BH as opposed to the case with gas content and without BH, where the gas density keeps increasing similar to the luminous matter density, forming a very dense clump in the center.

The measurable impact radius of the BH is much larger on the gas than on the luminous matter.

Line of Sight Density Profiles

Since observers can only measure line-of-sight profiles, the projected densities were plotted for the face-on and edge-on case regarding the gas disk. In figure 3.5 it becomes apparent that the visibility of the discussed features is dependent on the perspective. In the face-on case, the luminous density also becomes constant in the inner region for the BH-less galaxy, whereas the hole in the gas disk stays visible. When seen edge-on, the central hole is obscured but the luminous matter density

feature stays apparent even though it is somewhat damped.

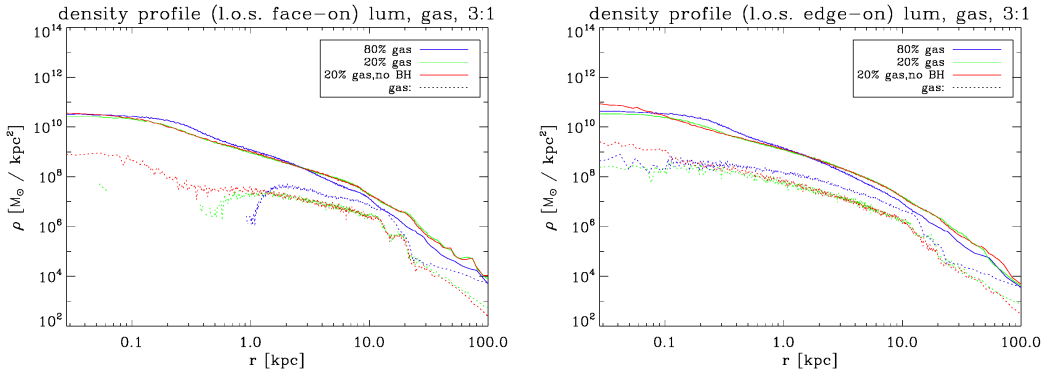

(a) The disk is viewed face-on. **(b)** The disk is viewed edge-on.

Figure 3.5: The density profiles of luminous and gaseous matter in the 3:1 mergers for two line-of-sight projections, one where the gas disk is face-on, the other where it is edge-on.

A possible explanation for the observed influences is that the BH accreted a considerable amount of mass through merging. That led to the release of feedback energy into the surrounding gas which consecutively got blown out. Through this effect, star formation is terminated in the central region resulting in a lower density (see Johansson et al., 2009b).

3.1.3 Mass Curves

A mass curve depicts the total mass inside a given radius. This cumulative mass of the luminous matter shows two distinct parts in all studied galaxies (fig. 3.6a for the 3:1 mergers). The outer part outside approximately 0.4 kpc (± 0.1 kpc dependent on the galaxy) has a relatively small slope that gets even smaller for increasing radii. Inside this radius the slope is significantly steeper. This characteristic is due to the fact that the density is decreasing for larger radii.

The peculiarity of the break is influenced by two factors. On the one hand, the curve becomes flatter on the outer part with a higher initial gas content because more mass is counted between about 0.5 and 10 kpc. This indicates that the newly formed stars are mainly located inside this region. On the other hand, the curve is steeper on the inner part if a BH is present. The BH indirectly reduces the luminous mass there by suppressing star formation.

There is no measurable direct influence of the BH on the star distribution as figure 3.6b shows. Here the newly formed stars were left out, so only the residual stars, i.e., the disk and the bulge particles, were taken into account. Since the red (no BH) and green (with BH) lines are identical now, the BH had no impact on the residual stars.

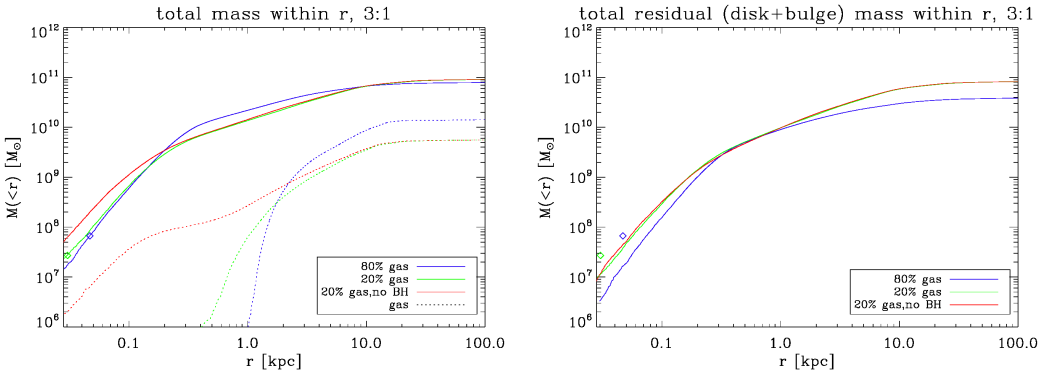

(a) Luminous and gas particles. **(b)** Residual (disk + bulge) particles only.

Figure 3.6: Cumulative mass curves for different sets of particles in the 3:1 mergers. The cumulative masses for the residual (disk + bulge) particles were calculated using the usual data but ignoring the newly formed star particles. Diamonds mark the dynamical ranges of the BHs and their masses.

One possible way to explain this is to calculate the dynamical range $r_{d,BH}$ of the BH (see table 3.1). The mass inside $r_{d,BH}$ equals the BH mass, so particles inside $r_{d,BH}$ are dynamically dominated by the BH. Since the $r_{d,BH}$ are close to the numerical resolution $\epsilon = 0.028$ kpc, especially in the 3:1, 20% gas simulations, a possible direct impact on the residual stars can not be resolved. Diamonds mark the BH mass and the according $r_{d,BH}$ in the plots.

Figure 3.6a also shows the cumulative gas mass as dashed lines. A feature that was already seen in the previous sections is that there is no gas inside a certain radius $r_{hole} \approx 1$ kpc because the BH feedback created a hole. The amount of missing gas was graphically estimated by reading off the total mass at r_{hole} for the case that no BH was present. The procedure was detailed in section 2.2.3 and is depicted in figure 3.7a and 3.7b. The results are summarized in table 3.1.

Apart from the 3:1, 20% gas simulation all gas curves for the BH-less case had to be guessed, which is very difficult, so they can only be seen as very rough first approximations. The missing gas masses m_{miss} equals between 5 to 15 times the BH mass, which is not a very big range considering the measuring method.

3.1.4 Rotation Curves

Rotation curves are used to connect the rotation velocity of a galaxy with its mass distribution. The rotation curves for the 1:1, no bulge and the 3:1 simulations are displayed in figures 3.8b and 3.8a, respectively. There is a strong peak around 0.3 - 0.7 kpc that is related with the original gas content. The 1:1, 0% gas case (3.8b, red) shows no peak, which leads to the conclusion that the other galaxies are dominated

Model	$M_{BH}[10^7 M_\odot]$	$r_{d,BH}$ [kpc]	r_{hole} [kpc]	$m_{miss}[10^8 M_\odot]$	m_{miss}/M_{bh}
11B2Bu	4.6	0.06	1	(5)	(10)
11B2nBu	9.1	0.05	2	(7)	(7)
31B8Bu	6.7	0.5	1	(10)	(15)
31B2Bu	2.7	0.03	0.5 - 1	1.4 - 2.7	5 - 10
ESp2	5.0	0.04	0.6	(2)	(4)

Table 3.1: Summary of calculated and estimated data. M_{BH} is the BH mass; $r_{d,BH}$ is the calculated dynamical range of the BH; r_{hole} is the approximated radius of the hole in the gas disk; m_{miss} is the approximated amount of gas missing in the hole

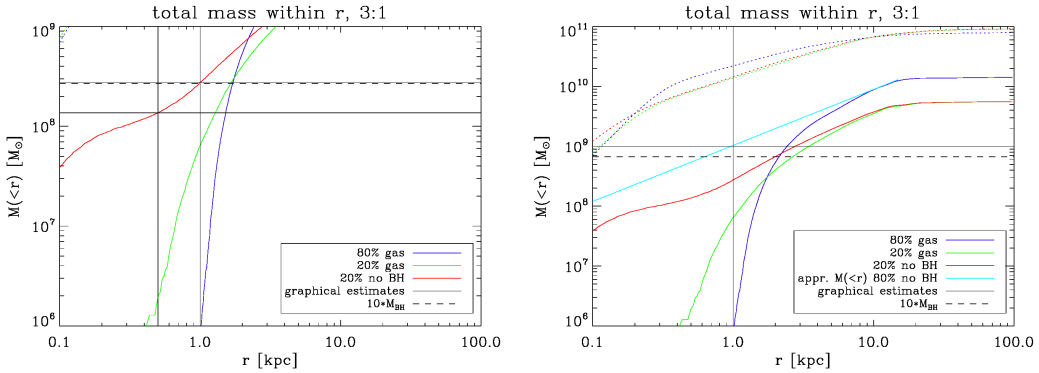

(a) Estimation for the 3:1, 20% gas merger. The plotted range is reduced and the gas curves are not dashed to improve accuracy.

(b) Estimation for the 3:1, 80% gas merger. The gas curve had to be approximated because the data was not available.

Figure 3.7: Graphical estimates of the gas masses that were removed by the BH in the 3:1 mergers. The amount of missing mass is about ten times the mass of the BH.

by new stars that formed in this region. The influence of the BH is again to reduce star formation inside 0.1 kpc, so the rotation curve is lower in the center and the peak is pointier.

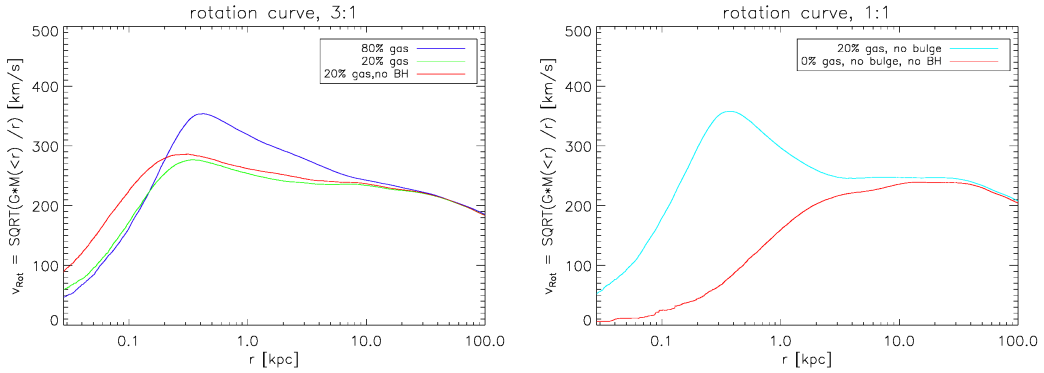

(a) 3:1 mergers.

(b) 1:1 mergers without bulge component.

Figure 3.8: Rotation curves calculated from all matter in the galaxies for 1:1 and 3:1 mergers. $v_{rot}(r) = \sqrt{GM(<r)/r}$ (see eq. 2.4).

A shallow, broad bump from about 2 to 5 kpc can be seen in the 3:1 mergers that is missing in the 1:1, no bulge simulations. This confirms that the initial bulge component did not move significantly from its original position. The same is true for the dark matter halo that is responsible for the flat part of the curve outside 5 kpc.

3.2 Dynamical Properties

An elliptical galaxy is not only defined by the distribution of its mass, which was discussed above. The dynamical properties of the matter also play an important role for the analysis of the galaxy and its interaction with the central BH.

3.2.1 Velocity Dispersions

One important parameter of the dynamical properties in a elliptical galaxy is the velocity dispersion. If plotted against the radius it can indicate the location of turbulences. The velocity dispersion profiles (fig. 3.9) are relatively linear outside 1 kpc. In logarithmic plots this suggests an underlying exponential distribution.

A distinct feature in galaxies with BH can be found at about 0.2 - 0.5 kpc, for each galaxy at exactly the same radius where the rotation curve had it's new stars peak. At these radii the velocity dispersion has a downward peak. This indicates that newly formed stars reduce the dispersion. This assumption is supported by figure 3.10, where the velocity dispersion of the luminous matter excluding new stars was

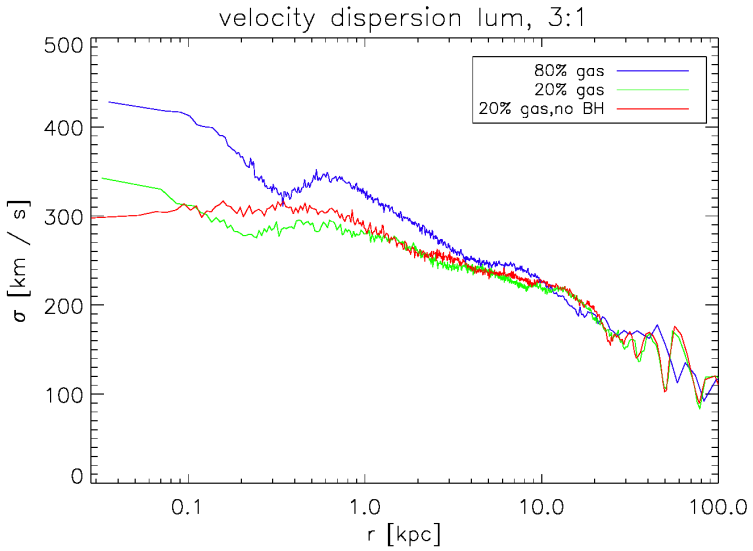

Figure 3.9: The velocity dispersion profiles of the 3:1 mergers for luminous and gaseous matter.

calculated. Here the drop vanishes and also the dispersion for the 3:1, 20% gas, no BH (red line in 3.10) does not become constant towards the center, as it did when newly formed stars where included.

Once more the indirect influence of the BH can be identified. By suppressing star formation in the center, the BH prevents the velocity dispersion from being flattened at small radii. The dump in the new stars dominated region when a BH was present could imply that the BH enhances star formation around 0.5 kpc.

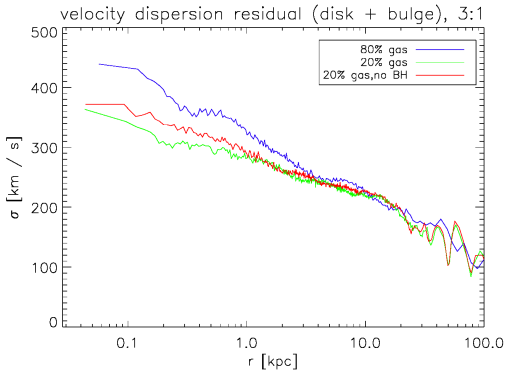

Figure 3.10: The velocity dispersion profiles of the residual stars in the 3:1 mergers.

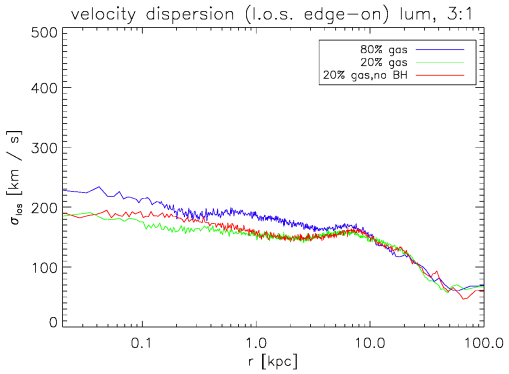

Figure 3.11: The velocity dispersion profiles of the luminous matter in the 3:1 mergers in the line-of-sight projection where the gas disk is edge-on

Line of Sight Velocity Dispersion

The line-of-sight (l.o.s.) velocity dispersion is a common observable. Therefore, it was also examined in this work. The dispersion is generally much smaller and almost constant around 200 km/s over a large range (fig. 3.11). This is in good agreement with usually observed values (Binney and Tremaine, 2008, p. 352). Unfortunately, the features seen in the intrinsic plots (fig. 3.9) vanish almost completely, especially in the face-on projection. A reason for the latter seems to be that the velocity components of the newly formed stars perpendicular to the gas disk are smaller than those in the disk plane. Only in the edge-on projection the drop around 0.2 kpc can be seen, but it is very faint.

3.2.2 Anisotropy Parameters

The anisotropy parameter $\beta = 1 - (\overline{v_\theta^2} + \overline{v_\phi^2})/(2\overline{v_r^2})$ (see eq. 2.3) characterizes the radial anisotropy of a galaxy. It's profile in the 3:1 and E-Sp mergers is shown in figures 3.12a and 3.12b respectively. Despite a feature at about 10 kpc, the parameter is in principle close to 0 all the way out to approximately 20 kpc. This means that the galaxies are isotropic and well mixed in this range. Further out, β turns positive indicating a radial bias and the border of the luminous galaxy.

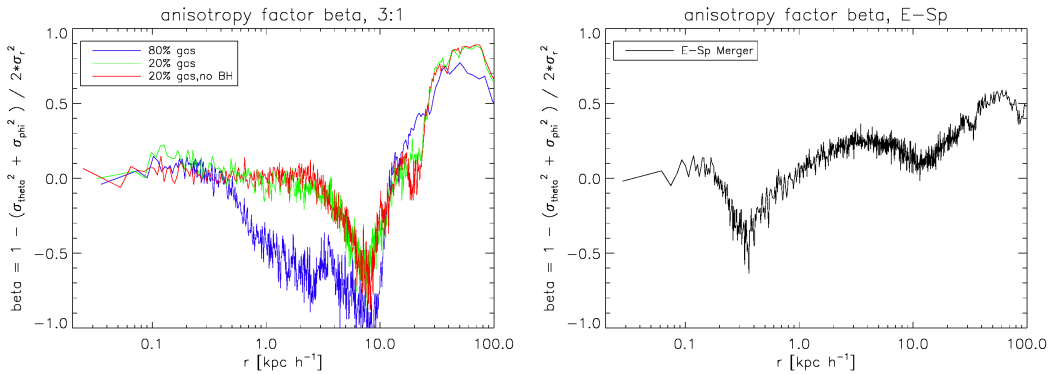

(a) 3:1 mergers. **(b)** E-Sp merger.

Figure 3.12: The radial anisotropy parameters $\beta = 1-(\overline{v_\theta^2}+\overline{v_\phi^2})/(2\overline{v_r^2})$ of the luminous matter in the 3:1 and the E-Sp mergers.

In the 3:1 simulations (fig. 3.12a) there is a strong negative peak between 5 - 10 kpc, which is strongest and broadest in the 80% gas case. This is due to a ring of rotating stars that survived the merging and is further enhanced by the newly formed stars. The same effect is noticeable in the E-Sp simulation (fig. 3.12b), but at a smaller radius of 0.5 kpc and a little less pronounced. That is because the galaxy is more massive and thus harder to disturb.

There is no resolvable influence of the BH as was expected from its small dynamical range.

3.3 Gas Disk Properties

The influence of a BH on an elliptical galaxy occurs to a significant extend through interaction with the gas. Therefore it is interesting to take a look at the properties of the gas disk.

3.3.1 Rotation, In- and Outflow

First, the radial component of the velocity of the gas v_r was studied. If $v_r < 0$ the gas moves towards the center where also the BH is located, if $v_r > 0$ it moves away. Figure 3.13 displays the projected velocities of the gas particles in the inner 0.5 kpc. The projection planes are again defined by the principal axes of the luminous matter (sec. 3.1.1). All particles rotate in the same sense around the center and stay principally in the disk plane.

In the upper left panel of figure 3.13 there is a pattern of alternating colors between red and blue. The blue arrows represent gas with $v_r < 0$, the red have $v_r > 0$. The gas has a velocity component towards the center in the upper right and the lower left part. It drifts away from the middle in the upper left and lower right. This reveals that the particles are rotating on elliptical orbits within the disk. For perfectly circular orbits, v_r would be vanishing everywhere. On an elliptical orbit there are two points where the distance to the center is largest.

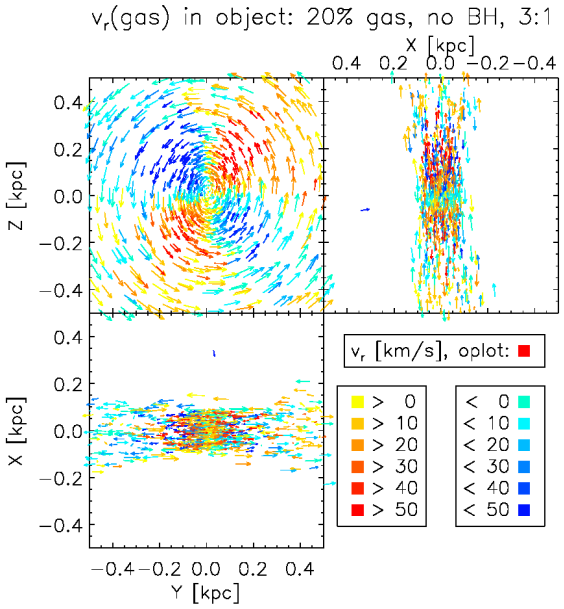

Figure 3.13: The projections of the gas particle velocities in the inner 0.5 kpc of the 3:1, 20% gas merger without BH. They are colored blue if they have a velocity component towards the center, and red if they move away from the center.

In the upper left panel of figure 3.13, all these points lie on the vertical axis. From there they move counter-clockwise towards the point of minimal radius, on the horizontal axis in the picture. To do that they must have a velocity component $v_r < 0$ towards the center, so they are plotted in blue. From there they again move out on their elliptic orbits, resulting in $v_r > 0$ and the red plot color.

The projected mass distributions (sec 3.1.1) already indicated the same ellipticity for the luminous matter. This suggests that the gas follows the potential of the stars because there is much more luminous than gaseous matter.

The elliptic orbits can be found in the whole gas disk as shown in figures 3.14a and 3.14b. Both figures show the 3:1, 20% gas simulation with BH at distances up to 10 kpc, but in the first figure the blue vectors where plotted on top of the red ones, and in the second figure vice versa. This is necessary because in some areas they cover each other. The color pattern is a bit more complicated than in the previous case of figure 3.13, but has the same reason.

The first panel in figure 3.14a shows the gas with a velocity component towards the center (blue) in the lower left and upper right corner. Figure 3.14b clarifies that the gas that moves away from the center (red) is concentrated towards the upper left and lower right. This pattern is explainable by elliptical orbits around the center, as it was indicated before (fig 3.13)

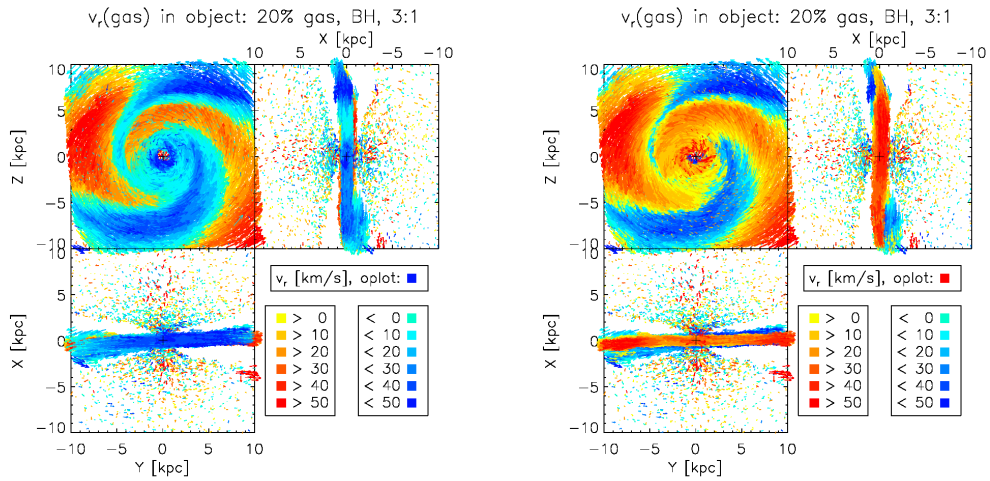

(a) The blue vetors are plotted over the red ones.

(b) The red vetors are plotted over the blue ones.

Figure 3.14: The projected gas particle velocities in the inner 10 kpc of the 3:1, 20% gas merger with BH. They are identical except for the sequence of the plotted vectors. The vectors are blue if the particles move towards the center and blue if they move away.

The projections of the gas particle velocities in the central 0.5 kpc of the 3:1, 20% gas merger without BH. They are colored blue if they have a velocity component towards the center, and red if they move away from the center.

Figure 3.14b (10 kpc) also indicates another influence of the BH. There are many red arrows close to the center and perpendicular to the disk plane. They symbolize particles that move away from the center with a v_r greater than 50 km/s. Nevertheless, the projected component in the disk plane is still larger that the one perpendicular to it. An explanation for this observation is that the interaction with

the BH accelerates the gas, that still has angular momentum. Therefore the gas escapes in a cone-shape perpendicular to the disk. Only there it does not collide with other gas particles in the disk plane.

This interpretation is also supported by the 3:1, 80% gas, with BH simulation (fig. 3.15a). Due to the higher gas fraction and the more massive BH, the feedback is bigger, so more and faster particles are ejected. The central gas hole is also more massive then for the same reason.

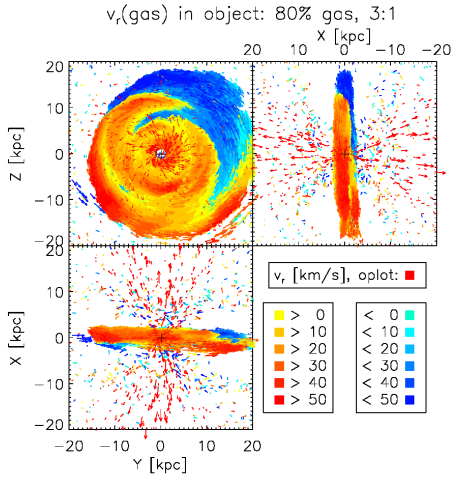

(a) The inner 20 kpc of the 3:1, 80% gas merger.

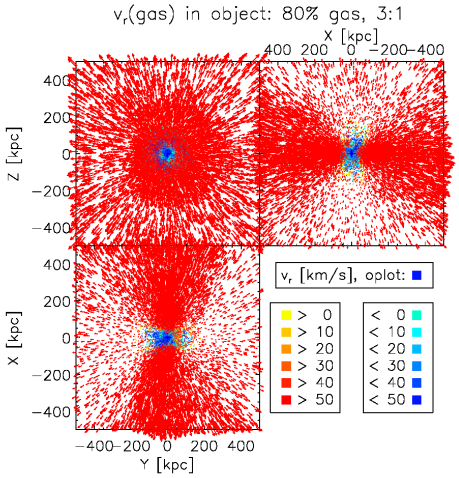

(b) The inner 500 kpc of the 3:1, 80% gas merger. The cold gas (blue) in the center indicates the size of the galaxy.

Figure 3.15: The projected gas particle velocities in the inner 20 and 500 kpc of the 3:1, 80% gas merger with BH. Note the high velocity particle outflow from the center on both scales, plotted in dark red.

Figure 3.15b displays the same as figure 3.15a but covering much bigger distances up to 500 kpc. It shows that there is a strong axial outflow from the disk. In all simulations only outflowing gas with high velocities can be found outside 200 kpc, so the gas mass $m_{r>200kpc}$ outside this radius was calculated and is summarized in table 3.2.

The mass that is missing in the central hole coincides with the mass that is escaping the galaxy as indicated by $m_{r>200kpc}/m_{miss} \approx 1$. Only in the 3:1, 80% gas and the E-Sp mergers about 3 times as much gas is moving away, which suggests that the general diffusion of hot gas away from the disk also plays a role for the removal of gas. This is also supported by the fact that in the 3:1, 20% gas simulation without BH there is also an outflow of gas, but with only 1/3 of the mass of the simulation with BH. Thus the anisotropy in figure 3.15b (500 kpc) can be understood as a shadow of the disk for diffusing gas.

Model	$M_{BH}[10^7 M_\odot]$	$m_{r>200kpc}[10^8 M_\odot]$	$m_{r>200kpc}/M_{BH}$	$m_{r>200kpc}/m_{miss}$
11B2Bu	4.6	7.1	15.4	(1.4)
11B2nBu	9.1	8.3	9.2	(1.2)
31B8Bu	6.7	35.9	53.6	(3.6)
31B2Bu	2.7	2.4	9.0	1.7 - 0.9
31nB2Bu	0	0.8	-	-
ESp2	5.0	10.1	20.1	(2.5)

Table 3.2: Relations of the mass escaping from the galaxy outside 200 kpc ($m_{r>200kpc}$) to the mass of the central BH M_{BH} and to the amoung of gas that is missing in the center (m_{miss}).

3.3.2 Temperature Distributions

The temperature distribution of the gas can give an explanation for the result above that gas particles are driven away from the galaxy.

Phase Diagram

One way to study the temperature distribution is to plot it against the density ρ of the gas particles in a phase diagram. The phase diagrams for the 3:1, 20% gas mergers (fig. 3.16a and 3.16b) are very similar at temperatures around 10^4 K and densities around $10^6 M_\odot/kpc^3$. This is the domain of the cold gas and it contains the most particles. The gas was efficiently cooled down to 10^4 K by radiative cooling, that is the energy loss of gas clouds through photon emission of particles that were excited by collisions. But below 10^4 K this process gets inefficient. The gas can only cool down further by adiabatic cooling, a process in which internal energy is reduced by expansion. That is why the coldest gas in the figures can be found towards low densities.

The branch towards higher densities and temperatures is typical for star formation. Cool and dense gas causes a lot of star formation which generates super novae (SN). The feedback of these events then heats up the gas. As seen in the density plots (sec. 3.1.2) the BH reduces the density in the central region, so the star formation branch in fig 3.16a is shorter here. The density reaches very high values in the 20% gas, no BH galaxy (fig 3.16b, so the heating from SN feedback is very strong there and the branch is longer.

The feature in the upper left parts of the figures is gas in a hot phase that escaped from the high density region of the gas disk. After escaping, it could start to expand and to cool down because the SN rate decreased and reduced the heating.

The impact of the BH is to blow out gas particles from the center, where their density would be highest. They get heated into the hot phase by the BH feedback, where star formation is suppressed.

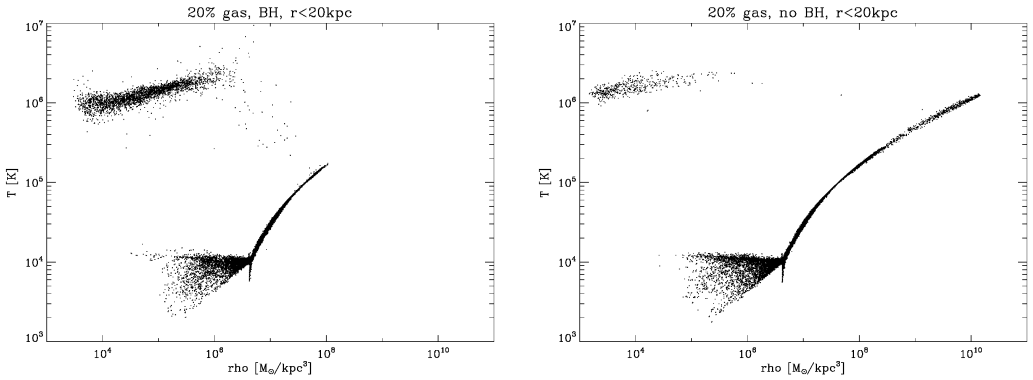

(a) 3:1,20% gas merger with BH. **(b)** 3:1,20% gas merger without BH.

Figure 3.16: The temperature-density scatter plots of the 3:1, 20% gas mergers with and without BH. Only the gas particles in the inner 20 kpc were considered. rho is the density of each particle, which was read out directly from the raw simulation data.

Spatial Distribution

The spatial distribution of the gas temperatures in the disk is shown in figure 3.17 for the 3:1, 20% gas merger with a BH. Gas below 10^4 K is called cold and is blue here, and gas above the threshold is called hot and is drawn in red. There is a ring of cold gas in the outer parts of the disk. The coldest parts below $5 \cdot 10^4$ K are in the outer tidal tails where the density is lowest. Therefore star formation and its SN feedback heating is low, so cooling below 10^4 K by adiabatic expansion is possible. The gas gets the hotter the closer it is to the center.

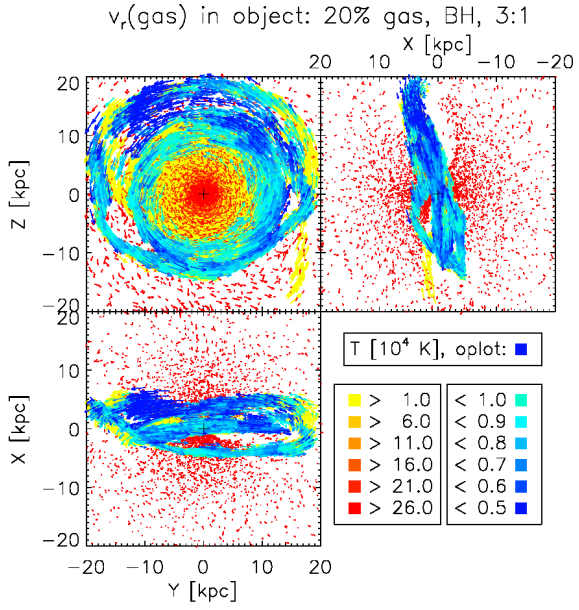

Figure 3.17: The projected gas temperature distribution in the inner 20 kpc of the 3:1, 20% gas merger with BH. The velocity vectors of cold gas particles below the threshold of 10^4 K are plotted in blue, those of hot gas in red. The bin sizes for hot and cold gas are not the same. Here, the blue colors are plotted over the red ones.

A more detailed temperature structure of the 3:1, 20% gas simulations inside 5 kpc is illustrated in figures 3.18a and 3.18b. The first is the zoom-in of the above plot and has a central BH, the second has no BH. Both show a very similar temperature gradient towards the center. This can be explained through the fact that the densities increase similarly towards the center (see sec 3.1.2). Because of the high density of the relative cold gas, there is a lot of star formation which in turn heats the gas through its SN feedback.

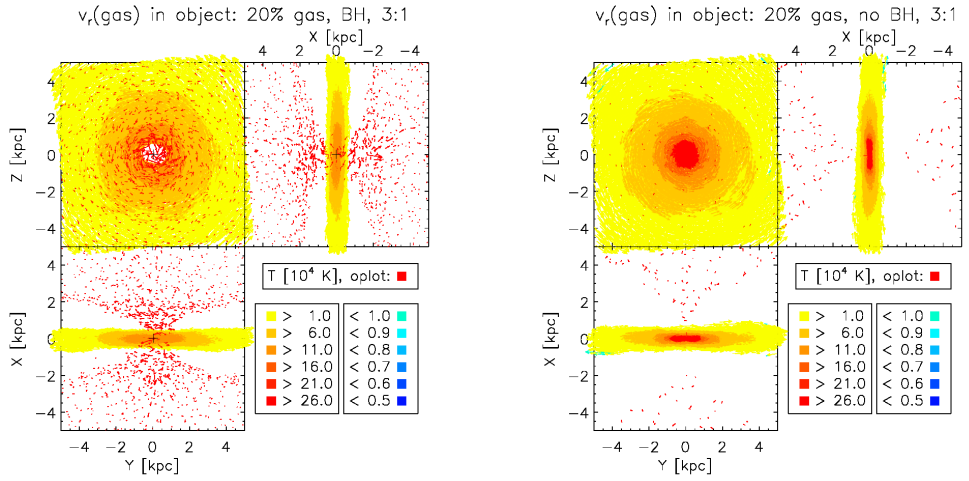

(a) 3:1, 20% gas merger with BH. **(b)** 3:1, 20% gas merger without BH.

Figure 3.18: The projected gas temperature distribution in the inner 5 kpc of the 3:1, 20% gas merger with and without BH. There are no gas particles in this region that are colder than 10^4 K.

By comparing these two figures, another impact of the BH can be seen. On the one hand the BH-less simulation in figure 3.18b only ejected a few hot particles from the center, so much more gas is still there. On the other hand, when a BH is present (fig. 3.18a), considerably more hot gas is outside the disk. The reason for this seems to be the combination of the changed potential in the center and the additional energetic feedback from accretion on the BH. This leads to an acceleration of the gas that is mainly visible if perpendicular to the disk where the particles can not collide with the disk.

For the 80% gas simulation, the ejection of hot gas is clearly recognizable even at a very large scale. Figure 3.19a shows the temperature distribution of this galaxy within a radius of 500 kpc. The outflow of hot gas and the shadow of the disk are clearly visible.

The equal mass mergers with gas content show similar features but they are a lot less pronounced because they do not have a very well defined gas disk. Especially in the 1:1 simulation with initial bulge component the gas is spread out isotropically and is relatively hot because the merger was more violent (fig. 3.19b). Only a vanishing fraction of the gas is colder than 10^4 K.

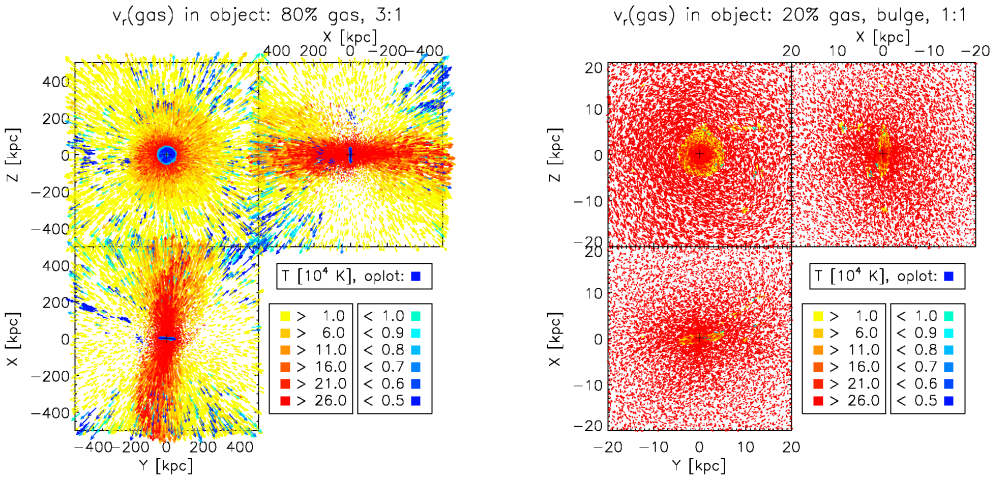

(a) The inner 500 kpc of the 3:1, 80% gas merger with BH. The cold gas (blue) indicates the size of the galaxy.

(b) The inner 20 kpc of the 1:1 merger with BH and bulge. There is almost no cold gas in this galaxy.

Figure 3.19: The projected gas temperature distributions in the inner 500 kpc of the 3:1, 80% gas merger with BH, and in the inner 20 kpc of the 1:1, 20% gas merger with BH and bulge component.

3.3.3 Star Forming Regions

The previous section indicated that there was a lot of star formation taking place. The fraction f_{conv} of gas particles that were converted into stars is given by $f_{conv} = N_{stars}/(N_{gas} + N_{stars})$, where N_{stars} and N_{gas} are the total numbers of new stars and gas particles in the galaxy, respectively. Table 3.3 shows that the values are indeed high. In the 3:1, 20% initial gas mergers 60% of the gas formed stars. If more gas was present or if the merger was more violent 70% - 80% of the gas was transformed.

Finally, the spatial distribution of the newly formed stars was studied. It is shown in figure 3.20a and 3.20b for the 3:1, 20% gas, with BH and without BH simulations,

Model No.	Mass Ratio	$f_{gas,init}[\%]$	f_{conv}
11B2Bu	1:1	20	68.9
11B2nBu	1:1	20	79.9
31B8Bu	3:1	80	73.1
31B2Bu	3:1	20	59.7
31nB2Bu	3:1	20	61.5
ESp2	E-Sp	20	75.9

Table 3.3: The fraction $f_{conv} = \frac{N_{stars}}{N_{stars}+N_{gas}}$ of gas particles that were converted into stars is high with ca 70%; N_{stars} is the total number of newly formed star in the galaxy, N_{gas} that of the gas particles

respectively, for distances up to 10 kpc. Here the red vectors represent the position and velocity of young stars that formed after the merger at approximately 1.5 Grys, and the blue vectors those of the old stars formed before merging. The distribution of young (red) stars follows the gas disk structure closely and they also rotate in the same way around the center. The density of recently formed stars increases towards the center similar to the temperature gradient discussed in the previous section 3.3.2.

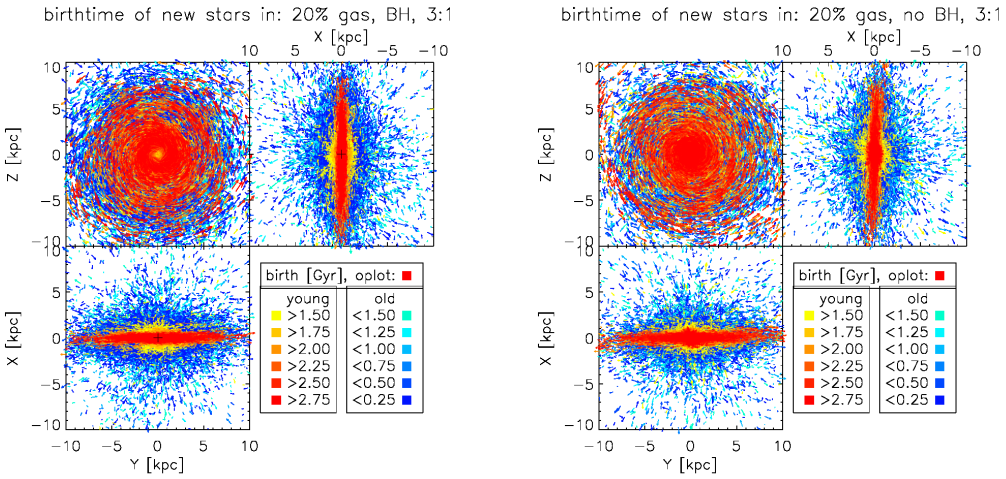

(a) 3:1, 20% gas merger without BH. Note the small area in the center of the galaxy without recently formed star.

(b) 3:1, 20% gas merger without BH.

Figure 3.20: The projected distributions of newly formed stars in the inner 20 kpc of the 3:1, 20% gas merger with and without BH. The stars that recently formed are called young and are plotted in red, whereas the stars that formed long before the merger are named old and are plotted in blue.

If the galaxy has a central BH (fig. 3.20a), the star formation is terminated for small radii below 1 kpc since the merging event. The reason for this is that the BH feedback blew away all the gas in this rather small area creating a hole in the gas disk. Due to the lack of gas, no new stars can form in the center.

If no BH was present (fig. 3.20b), star formation peaks in the center of the galaxy, leading to a slightly spherical distribution for very small radii that might be the first stage of a developing bulge.

The distribution of the stars that formed before 1.5 Gyrs (blue vectors in fig. 3.20a, 3.20b) is more chaotic and spread out, following the elliptical distribution of the other luminous matter. This is because the violent merger disturbed the orbits of the stars and forced them on more elliptical orbits.

4 Conclusion

This thesis examined the influence of central supermassive black holes (BHs) on the luminous and gaseous matter in major merger remnants. Johansson et al. (2009a) presented the high resolution simulations of the unequal and equal mass mergers that were used in this work. The simulations of elliptical galaxies with and without BHs were analyzed and compared in order to see differences in the properties of the stellar and gas components. For that, several aspects of the radial mass distribution and the dynamical properties were examined. These indicate that most of the BH's influence is on the gas, therefore the properties of the gas disks were also analyzed.

Due to the weak direct interaction with the luminous matter the available set of simulations turned out to be not optimal for the investigation of the influences of the BH. Of all simulations without BH, only the 3:1, 20% gas merger contained gas, therefore it is the most suitable for the comparisons. Still, the other simulations not only support the results but often provide additional information.

This work finds that the most significant influence of the BHs on the galaxies is, that they blow away the gas from the central region, so that there is a hole in the central gas disk with a radius of 0.5 - 1 kpc. The reason for this is, that the accretion of gas onto the BH during the merger causes so much energetic feedback that the surrounding gas is heated and accelerated to such a degree that it can potentially escape from the galaxy. The consequence is that no more new stars can form in this region. Thus the BH also changes the luminous matter distribution, but only in an indirect way by suppressing star formation in the center of the galaxy.

Evidence for the changed stellar distribution is found in several properties of the elliptical galaxies. Particularly pronounced features that can indicate the presence of a BH are found in the intrinsic density and velocity dispersion profiles. So with the knowledge of the influence of a BH on these properties, a determination whether a given galaxy contains a BH or not should be relatively easy. But in astronomical observations not the intrinsic but only projected density and velocity dispersion of galaxies can be measured.

Unfortunately, the peculiarity of the features in the line-of-sight projections almost completely vanishes for the velocity dispersion profiles and is strongly dependent on the given line of sight for the density profiles. There are indications that the presence of a BH can only be detected by the luminous matter distribution if it is known that the line of sight lies in the plane of the gas disk.

This means that the detection of a BH in an elliptical galaxy is difficult even in theory if only projected data are available. The influences of the BH on the intrinsic properties discussed here are found to be much more pronounced. Therefore if an observer could see the 3-dimensional structure of a galaxy, he could detect properties

of a BH.

A possible way to extract the unprojected structure from observed elliptical galaxies was examined by Thomas et al. (2004). They fit observational data to existing theoretical models to determine the intrinsic properties of the galaxies. Therefore the results of the examination of the influence of BHs done in this thesis can either be used to provide another parameter for their fitting method, or can be used to indicate properties of a BH in the unprojected galaxies.

Another problem for observers might be the small radius of the impacts of the BH. The range in which the BH potential can directly influence individual particles was calculated to be only about 0.05 kpc. This is very close to the numerical resolution of the simulation, so a direct impact on the luminous matter can not be expected to be visible.

Other influences have a larger range however. The creation of a hole in the gas disk through BH feedback and the termination of star formation in the center change important characteristics of the gaseous and luminous matter inside radii from the center of up to 0.3 - 1 kpc. Although this is still a small distance to be detected in a nearby galaxy, it is considerably larger than the 0.05 kpc of direct influence of the BH.

Another feature of the gas distribution is visible on a much larger scale of hundreds of kpc. It is shown that hot gas escapes from the the galaxy. This seems to be correlated with the gas that is removed from the center by BH feedback. Therefore, this represents a possible way to measure properties of the BH without the need for the highest resolution observations. Yet, due to the lack of reference simulations that contain gas but no BH, it was not possible to find the exact correlations. Further analyses based on additional suitable simulation data are needed to examine possible relations of the mass of the BH, the gas content of the galaxy, and the amount of gas that is missing in the center, to the mass of gas that gets ejected from the galaxy.

Bibliography

Binney, J. and Tremaine, S. (2008). *Galactic Dynamics: Second Edition*. Princeton University Press.

Hernquist, L. (1990). An analytical model for spherical galaxies and bulges. *The Astrophysical Journal*, 356:359–364.

Hernquist, L. (1992). Structure of merger remnants. I - Bulgeless progenitors. *The Astrophysical Journal*, 400:460–475.

Johansson, P. H., Burkert, A., and Naab, T. (2009a). The Evolution of Black Hole Scaling Relations in Galaxy Mergers. *The Astrophysical Journal*, 707:L184–L189.

Johansson, P. H., Naab, T., and Burkert, A. (2009b). Equal- and Unequal-Mass Mergers of Disk and Elliptical Galaxies with Black Holes. *The Astrophysical Journal*, 690:802–821.

Kormendy, J. and Bender, R. (2009). Correlations between Supermassive Black Holes, Velocity Dispersions, and Mass Deficits in Elliptical Galaxies with Cores. *The Astrophysical Journal*, 691:L142–L146.

Kormendy, J., Fisher, D. B., Cornell, M. E., and Bender, R. (2009). Structure and Formation of Elliptical and Spheroidal Galaxies. *Astrophysical Journal Supplement Series*, 182:216–309.

Kormendy, J. and Richstone, D. (1995). Inward Bound—The Search For Supermassive Black Holes In Galactic Nuclei. *Annual review of astronomy and Astrophysics*, 33:581–+.

Monaghan, J. J. (1992). Smoothed particle hydrodynamics. *Annual review of astronomy and Astrophysics*, 30:543–574.

Naab, T. and Burkert, A. (2003). Statistical Properties of Collisionless Equal- and Unequal-Mass Merger Remnants of Disk Galaxies. *The Astrophysical Journal*, 597:893–906.

Springel, V. (2005). The cosmological simulation code GADGET-2. *Monthly Notices of the Royal Astronomical Society*, 364:1105–1134.

Springel, V. and Hernquist, L. (2003). Cosmological smoothed particle hydrodynamics simulations: a hybrid multiphase model for star formation. *Monthly Notices of the Royal Astronomical Society*, 339:289–311.

Thomas, J., Saglia, R. P., Bender, R., Thomas, D., Gebhardt, K., Magorrian, J., and Richstone, D. (2004). Mapping stationary axisymmetric phase-space distribution functions by orbit libraries. *Monthly Notices of the Royal Astronomical Society*, 353:391–404.

Acknowledgements

I wish to thank all the people that supported me during the work on this thesis.

I am especially grateful to Prof. Dr. Andi Burkert for providing me with this fascinating subject and for integrating me so a warm-heartedly into his research group. It is a real pleasure to be supported by such a kind man.

I also owe special thanks to my supervisor Rhea-Silvia Remus for her great support and her always open ear. She gave me a lot of good and helpful advise whenever i needed it.

Thanks are due to my girlfriend, family and friends for all their support during this sometimes difficult time. They always were of great help in many ways.

Selbstständigkeitserklärung

Hiermit versichere ich, dass ich diese Arbeit selbstständig verfasst habe. Ich habe keine anderen als die angegebene Quellen und Hilfsmittel benutzt, sowie Zitate kenntlich gemacht.
Mir ist bekannt, dass Zuwiderhandlung auch nachträglich zur Aberkennung des Abschlusses führen kann.

München, 19.7.2011